

# Analyzing the Impact of ISO on Digital Imager Defects with an Automated Defect Trace Algorithm

Jenny Leung<sup>a</sup>, Glenn H. Chapman<sup>\*a</sup>, Yong H. Choi<sup>a</sup>, Rohit Thomas<sup>a</sup>, Zahava Koren<sup>b</sup>, Israel Koren<sup>b</sup>

<sup>a</sup>School of Engineering Science, Simon Fraser University, 8888 University Drive, Burnaby, BC, Canada, V5A 1S6

<sup>b</sup>Dept. of Electrical & Computer Engineering, Univ. of Massachusetts, Amherst, MA, USA 01003

## ABSTRACT

Reliability of image sensors is limited by the continuous development of in-field defects. Laboratory calibration on 21 DSLRs has revealed hot pixels as the main defect type found in all tested cameras, with 78% of the identified defects having a time-independent offset. The expanded ISO range that exists in new cameras enables natural light photography. However, the gain applied to all pixels also enhances the appearance of defects. Analysis of defects at varying ISO levels shows that compared to the number of defects at ISO 400, the number of defects at ISO 1600 is 2-3 times higher. Amplifying the defect parameters helps differentiate faults from noise, thus detecting larger defect sets and causes some hot pixels to become saturated. The distribution of defect parameters at various ISO levels shows that the gain applied to faults with moderate defect magnitude caused 2-10% of the defects to saturate at short exposure times (0.03-0.5s). With our expanded defect collection, spatial analysis confirmed the uniform distribution of defects, indicating a random defect source. In our extended study, the temporal growth of defects is analyzed using our defect-tracing algorithm. We introduce an improved defect model which incorporates the ISO gain, allowing the detection of defects even in short exposure images at high ISO and thus providing a wider selection of historical images and more accurate defect tracing. Larger area sensors show more hot pixels, while hot pixel rates strongly grow as the pixel size decreases to 2.2 microns.

**Keywords:** defect detection, hot pixel, imager defects, active pixel sensor, APS, CMOS image sensor, demosaicing

## 1. INTRODUCTION

Digital imagers have become increasingly popular over the last decade and are the dominating imaging devices in our daily life as well as in many industrial applications. Digital imagers develop defects like all microelectronic devices; however, unlike faults in other digital products, most in-field defects in digital imagers are permanent and their number increases continuously over the lifetime of the sensor. Faulty pixels will degrade the quality of the image captured by the sensor. Although defects can be taken care of by factory calibration, this can be expensive and sometimes infeasible for imagers used in remote sensing applications. Therefore, the study of in-field defects can help identify the characteristics of the faulty pixels and pinpoint the in-field defect causal mechanism, thus helping in the development of a better defect correction method.

In our early work, manual calibration techniques were used to identify defects in numerous commercial cameras<sup>1</sup>. Results from the calibration have suggested that hot pixel is the dominating defect type found in most commercial cameras. In our most recent study, we have found more defects revealed when calibrated at higher ISO levels; hence the degradation of image quality due to defects is much more significant at high ISO settings. As sensor technology improves, effective sensor noise is reduced. This reduced noise and better amplifiers allow an expanded ISO range, which in turn permits more natural light photographs and reduces the use of flash and long exposures. However, amplification of pixel output at high ISO will enhance the brightness of defective pixels, further degrading the image quality. In Section 2 we discuss in detail the impact of ISO on hot pixel defects, and how a high ISO can provide a more accurate calibration result.

---

\* glenn@cs.sfu.ca; phone 1-778-782-3814; fax 1-778-782-4951; <http://www.ensc.sfu.ca/people/faculty/chapman/>; School of Engineering Science, Simon Fraser University, 8888 University Drive, Burnaby, BC V5A 1S6, Canada

In our continuing study of pixel defect development, we utilize quantitative details such as the spatial location and temporal growth of defects to gain insight into the defect source mechanism. Defect locations can be found using simple laboratory calibration. However, defect growth over time could, until recently, only be analyzed by manually searching through all images taken by the same camera, making it a very difficult and time-consuming process. In our previous studies<sup>2,3</sup>, we proposed a detection algorithm that utilizes Bayesian statistics to automatically detect the presence or absence of defects by searching through an image set. In a recent study<sup>4</sup> we showed that the visibility of defects changes at different ISO settings. In this paper we build on our previous results and introduce an enhanced pixel model that will provide a better estimate of the pixel status by incorporating the ISO gain factor. An overview of both the previous algorithm and the improved one is discussed in Section 3. We then use the algorithm to trace the defect growth rate in 6 cameras and compare the results to the manual calibration defect count. The improved algorithm allows us to trace and analyze the defect growth from a wider range of cameras with better accuracy, thus increasing the statistical relevance of our defect analysis. Section 4 deals with the effects of sensor size and pixel size on the defect density, and Section 5 concludes the paper.

## 2. EFFECT OF ISO ON HOT PIXELS

In our previous study<sup>5</sup>, we have performed manual calibrations on numerous commercial DSLRs. In particular, we used dark field exposure (i.e., no illumination) to test for stuck-high and partially stuck defects, and bright field (i.e., uniform illumination at near saturation) to test for stuck-low defects. However, in our experiments, we have not found any of these stuck defect types. Instead, hot pixels were the dominating defect type. A hot pixel has an illumination-independent component that increases linearly with exposure time. Hot pixels can be identified by capturing a series of dark field images at increasing exposure times. The dark response of a hot pixel is demonstrated in Figure 1 showing the normalized pixel illumination vs. exposure time (illumination level 0 represents no illumination and 1 represents saturation). The dark response of a good pixel should be close to 0 (with some variation due to noise in the sensor) at any exposure level, as shown in plot (a). Moreover, we have found<sup>5</sup> that hot pixels can be categorized into two types: standard hot pixels as shown in plot (b) which have an illumination-independent component that increases linearly with exposure time; and partially stuck hot pixels as shown in plot (c) which have an additional offset that can be observed at no exposure.

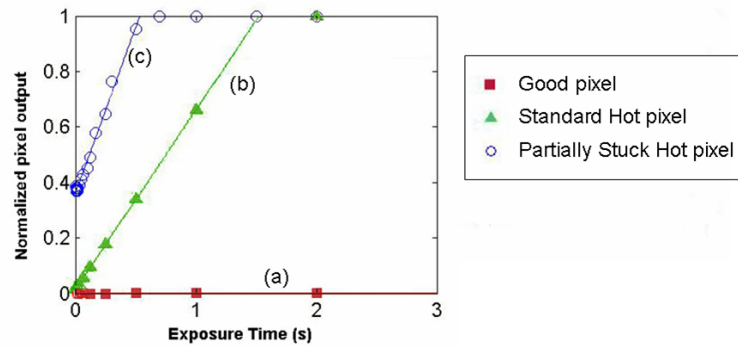


Figure 1: Comparing the dark response of a good pixel and a hot pixel.

A typical operation of a pixel can be modeled using Equation (1), where  $R_{photo}$  measures the incident illumination rate,  $R_{Dark}$  is the dark current rate,  $T_{exp}$  measures of the exposure setting,  $b$  is the dark offset, and  $m$  is the amplification from the ISO setting, which is directly proportional to the ISO setting.

$$I_{Pixel}(R_{photo}, R_{Dark}, T_{exp}, b) = m \cdot (R_{photo} T_{exp} + R_{Dark} T_{exp} + b) \quad (1)$$

In the case of a good pixel, both  $R_{Dark}$  and  $b$  are zero; therefore, the output from such a pixel is simply the measure of incident illumination. For a hot pixel, two more terms are added on top of the incident illumination; thus the output from such a pixel will appear brighter. The dark response of a pixel can be estimated by setting  $R_{photo} = 0$ , and Equation (1) is then simplified into

$$I_{offset}(R_{Dark}, T_{exp}, b) = m \cdot (R_{Dark} T_{exp} + b) \quad (2)$$

Based on Equation (2), the calculation of the dark response, also called the combined dark offset, of any hot pixel resembles a linear equation. By plotting the pixel dark response vs. exposure time, as shown in Figure 1, a linear

function can be used to estimate  $R_{Dark}$  and  $b$ . For a standard hot pixel  $b$  is zero, and therefore, this type of defects is most visible in long exposure images. For partially stuck hot pixels, on the other hand, the response depends on the magnitude of  $b$  and this type of defects will appear in all images.

To identify hot pixels in the set of dark field images, we used a threshold test to distinguish hot pixels from noise signals. The noise level in sensors varies and increases with the ISO level. To determine the threshold level used in our experiments we plotted the noise signal from various cameras as shown in Figure 2. The variation of noise levels at different ISO settings can be approximated using an exponential function shown in Equation (3). By taking the average of the A and B values, we get an approximate measure of the noise signal in these sensors; thus pixels with output three times higher than the noise signal are identified as defective.

$$y = A \exp(Bx), \quad \text{where } x = \log_2 \left( \frac{ISO_x}{50} \right) \tag{3}$$

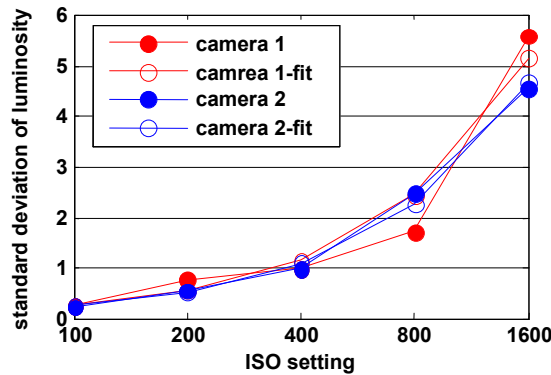


Figure 2: Dark noise signal from DSLR.

In our on-going study we have identified hot pixels from 21 DSLR cameras including both APS and CCD sensors, with the age of these cameras varying between 1 and 6 years. After performing the dark-frame calibration at ISO 400, the breakdown of the hot pixel types is summarized in Table 1. The results shown in Table 1 indicate that the majority of DSLR cameras will develop a significant number of hot pixels while operating in the field. In our most recent analysis, we have found 243 hot pixels of which 78% were of the partially stuck type. The offset in partially stuck hot pixels causes this type of defect to appear at any exposure level, which therefore has a greater impact on the image quality.

## 2.1 Impact of ISO on hot pixels

ISO setting is one of the most common functions used among photographers. It provides amplification of the pixel output, thus an object can still be captured even under low light conditions. The amplification level scales proportionally with the ISO setting, but the usable ISO range is limited by the noise level of the sensor. Before 2004, most commercial DSLRs had a usable ISO range of ISO 100 – 1600. As sensor technology improved, noise levels have been reduced and the usable ISO range has expanded. Some of the new DSLR models sold today have a usable ISO range of up to 25600. The ability to capture images at high ISO is a great benefit to photographers as it permits natural light photography without the need for flash or a long exposure setting.

In our previous analysis, we have performed all calibrations at ISO 400 as the noise level at this setting is very small in most cameras. However, observing Equation (1), the numerical gain that is applied to the pixel output amplifies the defect parameters as well. To observe the impact of ISO on defective pixels, we have performed the dark frame calibration at different ISO levels. Due to the increase of the background noise at higher ISO, the threshold value used to identify defects was adjusted according to Equation (3). Table 2 summarizes the results of our most recent calibration on a set of 13 DSLR cameras at varying ISO settings. As seen in Table 2, the number of identified defects increased as the ISO amplification increased. At ISO 400 we accumulated a total of 118 defects, and this almost doubled to 200 defects at ISO 800. At ISO 1600 we had a total of 292 defects, which is higher than the 243 defects identified at ISO 400 (see Table 1). This shows that at low ISO, many of the defects cannot be distinguished from

noise signals. By calibrating at higher ISO, defect parameters are being amplified as in Equation (2) and the distinction between noise and defect become clearer.

**Table 1: Summary of in-field defects from tested cameras at ISO 400.**

Camera	Sensor Type	# of pixels (MP)	Sensor size (mm)	Pixel size ( $\mu\text{m}$ )	Number of defects found		Total
					No offset	Hot W/offset	
A	APS	6.3	22.7 × 15.1	7.38 × 7.36	1	11	12
B	APS	21.0	36.0 × 24.0	6.26 × 6.26	0	7	7
C	APS	6.3	22.7 × 15.1	7.38 × 7.36	0	6	6
D	APS	12.2	22.2 × 14.8	5.14 × 5.14	0	2	2
E	APS	8.0	22.2 × 14.8	6.33 × 6.33	0	1	1
F	APS	12.2	22.2 × 14.8	5.14 × 5.14	0	2	2
G	APS	21.0	36.0 × 24.0	6.26 × 6.96	0	1	1
H	APS	8.2	22.5 × 15.0	6.30 × 6.30	0	4	0
I	APS	10.1	22.2 × 14.8	5.59 × 5.59	0	1	1
J	CCD	6.0	23.7 × 15.5	7.96 × 7.57	15	2	17
K	CCD	10.0	23.6 × 15.8	5.87 × 5.87	0	22	22
L	CCD	10.0	23.6 × 15.8	5.87 × 5.87	1	65	66
M	CCD	10.0	23.6 × 15.8	5.87 × 5.87	0	10	10
N	CCD	10.0	23.6 × 15.8	5.87 × 5.87	0	8	8
O	CCD	6.0	23.7 × 15.5	7.69 × 7.57	1	17	18
P	CCD	6.0	23.7 × 15.5	7.69 × 7.57	9	1	10
Q	APS	8.2	22.5 × 15.0	6.30 × 6.30	0	2	2
R	CCD	6.0	23.7 × 15.5	7.69 × 7.57	11	6	17
S	CCD	10.0	23.6 × 15.8	6.10 × 6.10	0	11	11
T	APS	12.2	23.7 × 15.7	5.39 × 5.38	0	0	0
U	CCD	5.3	23.7 × 15.5	7.87 × 7.90	18	8	26
<b>Cumulative total</b>							<b>243</b>

**Table 2: Summary of defect count at various ISO levels.**

Camera	ISO setting				
	100	200	400	800	1600
A	3	9	12	23	23
B	1	2	7	8	16
C	0	1	6	11	20
D	1	1	2	4	10
E	0	0	1	4	12
F	1	6	1	2	4
G	--	--	1	1	2
H	--	--	4	7	--
I	0	0	1	5	8
J	--	0	17	23	33
K	8	15	22	43	68
L	2	4	34	52	66
M	2	4	10	17	30
<b>Cumulative total:</b>	<b>18</b>	<b>42</b>	<b>118</b>	<b>200</b>	<b>292</b>

In Figure 3 we compare the dark response of an identified hot pixel at varying ISO levels. It is clear that at ISO 400, the defect has low values of  $R_{Dark}$  and  $b$ ; as the ISO amplification increases, both  $R_{Dark}$  and  $b$  increase dramatically. In fact, at ISO 12800 the dynamic range of the pixel is reduced by 20% solely due to the offset  $b$ , and at ISO 25600, the pixel is near saturation at all exposures. Given the high number of hot pixels with offsets this may suggest that the development of stuck high pixels in the field may actually be due to the presence of hot pixels with very high offsets.

This is consistent with our experience of never detecting a true stuck pixel in our cameras, but noting that there is mention of a few cameras developing stuck pixels in camera forums.

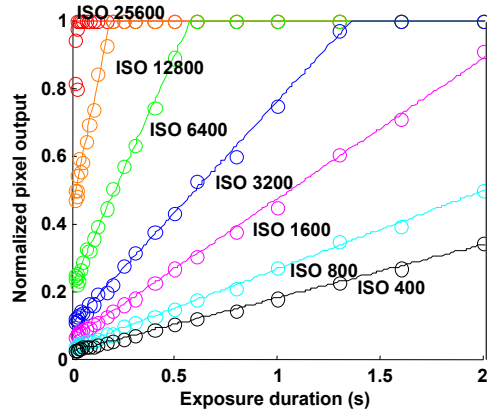


Figure 3: Dark response of a hot pixel at various ISO levels.

With the amplification from ISO, the  $I_{Offset}$  as calculated by Equation (2) dominates the illumination signal, causing further reduction in the pixel dynamic range. To see how the defect parameters vary over different ISO levels, we have plotted a histogram of  $I_{Offset}$  calculated at a common exposure of 0.5s (Figure 4(a)) and a long exposure of 1s (Figure 4(b)). In Figure 4(a) we can see that at 0.5s, most of the defects are low impact defects and have an  $I_{Offset}$  value below 0.1, but at ISO 400 about 10% of the defects will have an  $I_{Offset}$  of 0.2. With an ISO 1600, about 10% of the identified defects will saturate even at 0.5s. Looking at a longer exposure of 1s, as in Figure 4(b), we can see that the majority still has  $I_{Offset}$  below 0.1, but at the same time the number of pixels with  $I_{Offset}$  over 0.2 has increased by 20%. In fact, at ISO 1600, about 20% of the defects are at saturation. Pixels with an  $I_{Offset}$  of 0.2 will reduce their dynamic range by 20%. The important point here is that at high ISO settings there are considerably more observed hot pixels and they affect a wider range of exposure times.

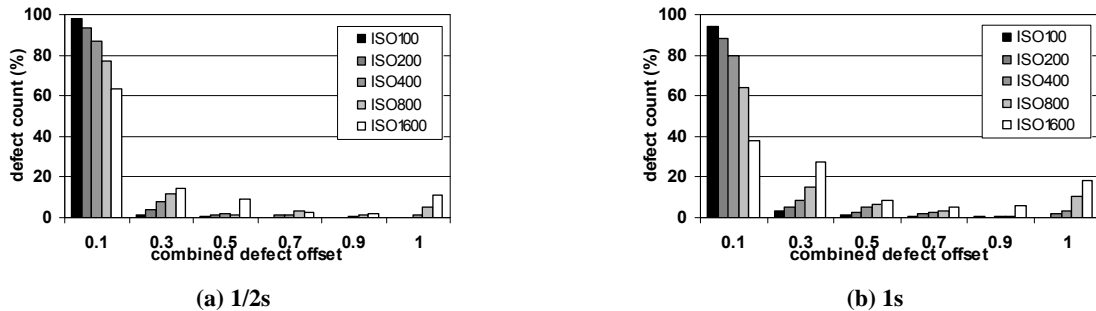


Figure 4: Histogram of  $I_{Offset}$  at varying ISO levels and two exposure times.

### 3. SPATIAL AND TEMPORAL DEFECT ANALYSIS

In our previous study, we used quantitative details such as the spatial distribution and temporal growth behavior of defects to gain conclusive insight into the physical mechanisms that are causing the in-field defects. In this section we extend this analysis to include the defects seen at higher ISO settings.

#### 3.1 Spatial distribution of hot pixels

Characteristics such as the spatial distribution can provide some insight into the causal mechanism of in-field defects. For defects related to material degradation, we would expect to observe local clustering of defects. On the other hand, defects caused by a random source such as radiation would develop randomly throughout the sensor. To answer the question – are hot pixels clustered or randomly distributed, we first calculated the Euclidean distance between all defects in each sensor. We then collected all these distances into the histograms shown in Figure 5. Since calibration

at higher ISO reveals more defects, we show the histograms for defects identified at ISO 400 (Figure 5(a)) and ISO 1600 (Figure 5(b)).

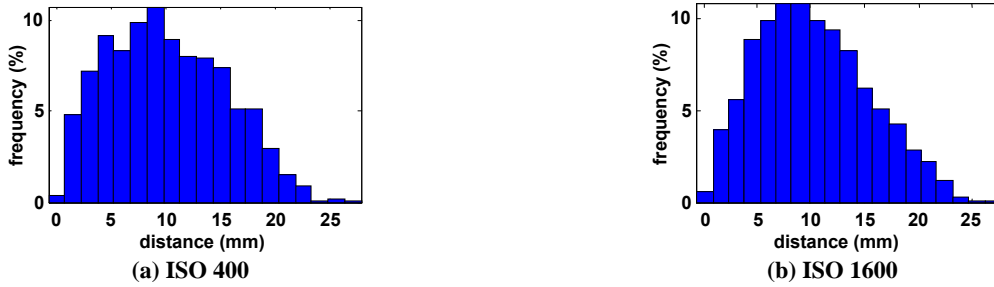


Figure 5. Spatial distribution of defect distances.

Despite having 3 times more defects found at ISO 1600 than at 400, both histograms display similar characteristics - a broad random distribution of the measured distances. If local clusters of defects existed in a sensor, we would expect to see multiple peaks at long and at short distances. The broad distributions that we see in Figure 5 with an average distance of about 10mm suggest that these in-field defects were caused by a random source such as radiation rather than by material degradation.

### 3.2 Temporal growth analysis using the defect trace algorithm

To track the defect growth rate of each individual camera, we need to obtain the actual development date for each defect. To this end, we use information from past images taken by the camera since each image captured is a record of the state of the sensor at the capture time. By searching through the entire image dataset of the camera, we can extract the time of the first appearance of each defect as shown in Figure 6. In the past, we performed this search using visual inspection of pictures, but this process is very slow and cumbersome when applied to a large collection of data. We later developed an automated defect trace algorithm for estimating the first appearance date of each defect, which we enhance in this paper to include the effect of the ISO setting.

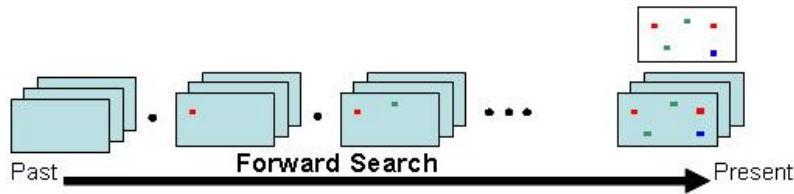


Figure 6: Defect trace algorithm.

In our algorithm, the imager is described by an array of  $W \times H$  pixels and the output at pixel location  $(i, j)$  is denoted by  $y_{ij}$ . In this algorithm, we will only focus on 8-bit RGB images; thus the image is composed of three color channels (Red, Green and Blue), each of which has an intensity between 0 (dark) and 255 (saturation).

Recall the mathematical model of a pixel in Equation (1). We can simplify it into Equation (4) where  $x$  measures the incident light that strikes the pixel, the defect parameter  $m \cdot (T_{exp} \cdot R_{Dark} + b)$  is denoted by  $\Delta$ , and  $m$  is the amplification due to the ISO setting. As discussed in Section 2.1, when a defect is calibrated at different ISO settings, both  $R_{Dark}$  and  $b$  are amplified as well. To compensate for the different ISO settings used in each image,  $m$  is calculated as a ratio factor, where  $ISO_x$  is the ISO setting of the current image and  $ISO_{calibrated}$  is the ISO setting used in the calibration.

$$y = m \cdot (x + T_{exp} \cdot I_{Dark} + b) = m \cdot x + \Delta, \quad \text{where } m = \frac{ISO_x}{ISO_{calibrated}} \quad (4)$$

The algorithm is executed on each camera separately. In the first step, dark frame calibration is used, as discussed in Section 2, to collect the spatial locations of the current hot pixels and the estimates of  $R_{Dark}$  and  $b$ . Next, for each image, we estimate the expected value of each pixel (denoted by  $z$ ) by interpolating the values of its neighboring pixels. The interpolation scheme we use here is averaging over the  $5 \times 5$  ring shown in Figure 7. The reason we do not average over the pixel's immediate neighbors is that digital cameras use a function called demosaicing, which interpolates the missing color channel at each pixel site. This process causes a single defective pixel to appear as a cluster of defects,

although these are not real hardware defects. By omitting the pixels from the  $3 \times 3$  region around the pixel, we overcome this problem and obtain a more accurate estimate of the pixel value. After calculating the image-wide interpolated values we compare them to the actual pixel values and obtain the image-wide interpolation errors. We next compute the interpolation error Probability Density Function (PDF) and Cumulative Density Function (CDF) denoted by  $p_E$  and  $P_E$ , respectively.

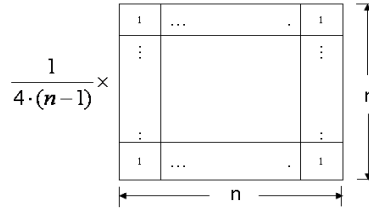


**Figure 7: Ring interpolation scheme.**

For each identified (in the first step of the algorithm) hot pixel, we move recursively forward in time over the images and use Bayesian equations to calculate the probability  $Prob(Good|y_k)$  that the pixel is good at the time when the  $k$ -th image was taken (where  $y_k$  is the pixel value in the  $k$ -th image). This probability will be close to 1 at the beginning (since the pixel was good when the camera was new) and will eventually go down to 0 as we move forward in time (since we know that it is now a hot pixel). For the first image where  $Prob(Good|y_k)$  falls below our predetermined threshold, we declare the date of this image as the defect development date. We use the following recursive Bayesian equations to evaluate  $Prob(Good|y_k)$ :

$$Prob(y_k | Good) = p_E(y_k - z_k) \quad (5)$$

$$Prob(y_k | Hot) = \frac{1}{255 - \Delta_{\min} + 1} \cdot [P_E(y_k - z_k - \Delta_{\min}) - P_E(y_k - z_k - 255)] \quad (6)$$

$$\Delta_{\min} = m \cdot ((I_{Dark})_{\min} \cdot T_{\exp} + b)$$

$$Prob(Good | y_k) = \frac{Prob(y_k | Good) \cdot Prob(Good | y_{k-1})}{Prob(y_k | Good) \cdot Prob(Good | y_{k-1}) + Prob(y_k | Hot) \cdot Prob(Hot | y_{k-1})} \quad (7)$$

$$Prob(Hot | y_k) = 1 - Prob(Good | y_k) \quad (8)$$

A typical plot of  $Prob(Good|y_k)$  over a sequence of images is shown in Figure 8. As can be seen, when the pixel is still good the value is  $\sim 1$  and it gets closer to 0 when the pixel becomes defective.

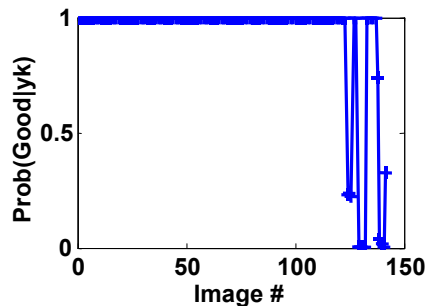


**Figure 8: Plot of  $Prob(Good|y_k)$  over a sequence of images.**

The appearance of hot pixels is affected by the exposure time and ISO setting used to capture the images. Low impact hot pixels are most visible in long exposures and high ISO settings, and can otherwise be hard to detect. An image of a busy scene or with a high ISO setting can result in large interpolation errors and false defect detection. To avoid such false detection we have proposed a correction scheme<sup>2</sup>. The final step of the algorithm is a correction step - for each image with  $Prob(Good|y_k) < threshold$  we calculate the local color variation of the small region around the defect. The variance in this local region indicates the accuracy of  $z$ . For a large variance, the detection is most likely caused by the interpolation error and the image is ignored.

### 3.3 Temporal growth of defects

We used the algorithm presented in the previous section on the image dataset of six cameras with age ranging between 2 and 5 years. The average size of the sensor in these cameras is  $23 \times 16 \text{ mm}$  and the average pixel size is  $6.5 \times 6.5 \mu\text{m}$ . With our improved calibration procedure, more defects were identified at high ISO. The following analysis is based on defects identified at ISO 1600. The six cameras we analyzed had a total of 65 defects. In our previous research<sup>2,3</sup> we tested various sizes of interpolation masks as shown in Figure 7, and the  $5 \times 5$  ring provided the best results. Therefore, we selected this ring for our experiments.

To determine the defect growth rate for each camera, we plot the number of identified defects vs. the camera age as shown in Figure 9, and the growth rate is estimated using a linear fit function. With the six cameras we have over 30,000 pictures, therefore it was not feasible to perform visual inspection of each image for testing the accuracy of the automated algorithm results. An alternative solution for testing our results was to utilize the defect count we obtained from manual calibration. For each of the cameras, we performed a dark frame calibration on a yearly basis; the defect count collected from these calibrations can provide an estimate of the growth rate of defects over the sensor lifetime. The growth rate results from both the defect trace algorithm and the calibration are summarized in Table 3.

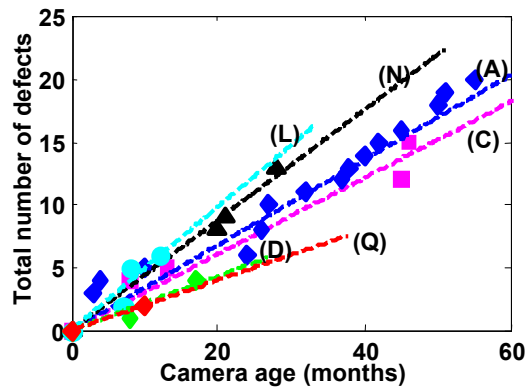


Figure 9: Defect growth rate (using the defect trace algorithm).

Table 3. Manual calibration and Bayes detection growth rate comparison at ISO 1600

Camera	Sensor Type	Sensor size (mm)	Sensor area ( $\text{mm}^2$ )	Pixel size ( $\mu\text{m}$ )	Defect growth rate		
					Manual calibration (defects / year)	Bayes detected (defects / year)	Error (%)
A	APS	$22.7 \times 15.1$	342.8	$7.38 \times 7.36$	5.38	4.18	22.0
C	APS	$22.7 \times 15.1$	342.8	$7.38 \times 7.36$	3.95	3.82	3.3
D	APS	$22.2 \times 14.8$	328.6	$5.14 \times 5.14$	2.58	3.01	14.3
L	CCD	$23.6 \times 15.8$	372.9	$5.87 \times 5.87$	5.92	5.88	0.7
N	CCD	$23.6 \times 15.8$	372.9	$5.87 \times 5.87$	4.97	5.27	5.7
Q	CCD	$22.5 \times 15.0$	337.5	$6.30 \times 6.30$	4.00	4.00	0.0

In Figure 9 we notice a similar linear increase in the number of defects in these cameras. The linear growth of defects suggests that in-field defects are not likely caused by a single traumatic event or material degradation. Material related defects will usually develop a cluster of spatially close defects at around the same time. However, our observed spatial distribution did not indicate any local clustering of defects. In fact, the shortest distance between two defective pixels was 2 pixels. The continuous increase in the number of defects observed in both types of sensors suggests that these sensors are continuously exposed to a similar kind of causal mechanism such as cosmic-ray radiation. This is consistent with similar conclusions in the literature<sup>6,7</sup>.

Comparing the defect growth rate detected using the continuous manual calibrations, the difference is less than the max error of 22%. The accuracy of the detection using historical photographs depends on the availability of images and the settings used for these images. For a user who does not capture photographs on a regular basis, the number of images used for analysis can be limited and the error can be large. Because the majority of photographs are captured at short

exposure times (~1/30s) and ISO setting below 800, low impact defects are barely visible in these images. Recalling the data in Figure 4(a), for images captured at 1/2s exposure time, only ~20% of defects will have  $I_{Offset} > 0.2$  at ISO 400. Thus, detection of low impact defects can be challenging, and in the worst case some defects may not be detected at all.

#### 4. SENSOR SIZE AND PIXEL SIZE

Another two major technological improvements in cameras is the increase of sensor size and increase of pixel numbers by decreasing the pixel size. However in this section we will show that, both these trends tend to increase the tendency to pixel defects.

##### 4.1 Impact of defects in larger area sensor

Another trend in higher end DSLRs is the increase in the sensor size to a full 36×24mm frame. Based on Table 1, camera B is an example of a full frame large area sensor that is about 1 year old. We performed two sets of calibration with this camera, the first calibration was done when the camera was just purchased and the second calibration was performed 9 months later. A second similar camera has been tested but has only one data set at this point and so is not included here. The calibration results are summarized in Table 4.

**Table 4. Defect count and growth rate for camera B.**

					Calibration Result		
Camera	Sensor Type	Sensor size (mm)	Sensor area (mm <sup>2</sup> )	Pixel size (μm)	First (2009-03)	Second (2009-11)	Growth rate (defects/year)
Camera B	APS	36.0 × 24.0	864.0	6.26 × 6.26			
@ ISO 400					0	7	9.3
@ ISO 1600					1	16	20.0

As expected, very few defects were identified by the first calibration at both ISO 400 and 1600. However, 9 months later our calibration has shown that a significant number of new defects have developed in the sensor. Calibration at ISO 400 has identified 7 defects and at ISO 1600 has identified 16 defects. The difference between the two defect counts indicates the defect growth rate for this camera as shown in the last column in Table 4.

The size of the sensor in Camera B is much larger compared to the three APS sensors we have analyzed in Table 3 (~23×15 mm), but the size of the pixels remains approximately the same. Based on defects identified at ISO 1600, the average defect growth rate of the APS sensors from Table 3 is ~3.67/year. If all cameras were exposed to the same radiation environment, we would expect the sensor with the largest sensing area to develop the most number of defects. The average area of the three APS sensors in Table 3 is ~338mm<sup>2</sup> which is only 40% of the sensor area in camera B (864mm<sup>2</sup>). Thus, we would expect camera B which has 2.5 times the sensing area to have a defect growth rate of ~9.17 defects/year. However, based on Table 4 the defect growth rate at ISO 1600 is 20 defects/year, which is significantly higher than our expected rate. Although the defect growth rate from Camera B is higher than expected, as some events such as the air flights with the camera (which exposes it to higher radiation) may cause a higher defect rate, a detail analysis with the defect trace algorithm is needed to find the exact time occurrence of these hot pixels. Certainly at this moment, with the same pixel size used in both large and medium area sensors, the high defect growth rate found in the large sensor indicates that the number of defects in the sensor is scaling at least with the total area of the sensor. As more new cameras will be using the larger area sensor, the impact of defects on the sensors will become more significant. The additional factor of much higher ISOs in these new cameras, as noted in section 2.1, will enhance this effect.

##### 4.2 Impact of small pixels on defect density

The number of pixels in an average commercial digital camera has increased from 3MP in 2002 to 12MP in 2009. In most cameras the size of the sensor remains the same but the size of the pixel is reduced; thus the number of pixel on sensor increases. In this study we have analyzed cameras from 10 cellphone of the same. The camera on these

cellphones uses a 5MP APS sensor with pixel dimension of  $2.2 \times 2.2 \mu\text{m}$ . The size of the pixels in these cellphone cameras is relatively small compared to a DSLR pixel, which is about  $6.47 \times 6.47 \mu\text{m}$ . By comparing the number of defects found in the cellphone cameras with the commercial DSLRs, and taking into account the reduced sensor area, we can gain insight into the impact of defects with reducing pixel size.

To identify defects from these cellphone cameras, the dark frame calibration procedure used for DSLRs cannot be applied because of the limited controls and functions available on these cameras. In particular, these cellphone cameras do not have explicit exposure control and therefore we cannot conclude whether an identified fault is a hot pixel or a stuck high defect. More importantly, these simple cameras do not provide the raw format function, and therefore all dark images are captured in color mode. Color images generated by digital cameras are often processed with various imaging functions such as demosaicing, noise reduction, white balance, and alike. These imaging functions tend to distort the faulty pixel, causing a single pixel defect to appear as a virtual cluster. To overcome these challenges we had to design a new procedure for calibrating these cameras.

First, a hot pixel is most visible in long exposure images; thus we utilize the exposure compensation setting to maximize the exposure time. Next, the ISO setting used in our calibration was ISO 400 as this is the highest level available on this camera. Finally, to ensure we can capture a dark image, the whole experiment was performed in a dark room condition. To identify defects from the calibration image, we applied a threshold test so that any pixel with an output value greater than the threshold was considered defective. Because defects are identified in color images, demosaicing will cause a single defective pixel to appear as a cluster pixels. Therefore, to achieve the best approximation of the exact defect location, each local cluster was considered as one defective pixel and by finding the peak output within the cluster we determined the exact location of the faulty pixel. Figure 10 shows an example of the local region of the one defect identified from our calibration. Plotting the three color planes separately, we can see this is a red defect and the single peak suggested the defect is located signal defective pixel.

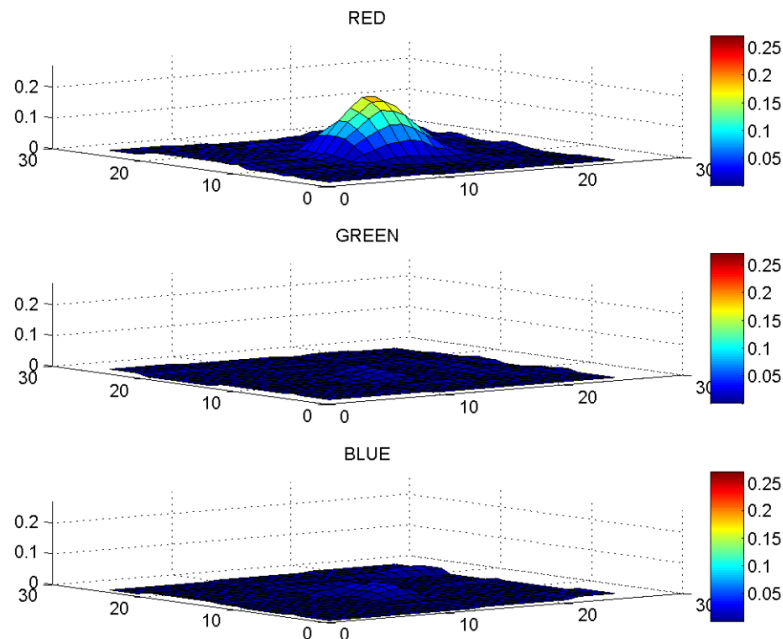


**Figure 10. Dark response of a defect identified from cellphone camera.**

To eliminate false detection due to noise, we captured a series of 3 sequential images for each camera and by taking the common result we obtained our final defect set from the cellphone. We have performed two sets of calibration on the cellphone cameras, the first when the cellphones were first received and the second 16 months later. The accumulated defect count from the two sets of calibration is summarized in Table 5.

Vcdig'70Ceevo wrcvgf 'f glgewult qo '32'egnrj qpg'eco gt cu0'

Cellphone	2008	2009
Cell A	9	21
Cell B	13	21
Cell C	8	19
Cell D	6	25
Cell E	12	24
Cell F	14	22
Cell G	14	21
Cell H	10	25
Cell I	14	25
Cell J	17	17
<b>Cumulative Total:</b>	<b>110</b>	<b>220</b>

As seen in Table 5, our first calibration identified a total of 110 defects in the 10 cellphone cameras. These cameras are an embedded device in the cellphone, and the mapping of manufacture time defects is not feasible for cost reasons as it is in commercial digital camera. Thus, the defects found in our first calibration may include manufacture time defects plus those developing before the test. Despite the lack of defect mapping from the manufacturer, in our second calibration (16 months later) the cumulative total has doubled to 220 defects. Taking the average number of identified defects per cellphone camera for each calibration, we have calculated the average defect growth rate for the cellphone cameras is 8.3 defects/year as shown in Table 6.

**Table 6. Average defect count and growth rate of 10 cellphone cameras.**

					Calibration Result		
Camera	Sensor Type	Sensor size (mm)	Sensor area (mm <sup>2</sup> )	Pixel size (μm)	First (2008-07)	Second (2009-11)	Growth rate (defects/year)
Cellphone @ ISO 400	APS	5.4 × 4.28	23.11	2.20 × 2.20	11	22	8.3

As shown in Table 6, the sensor used in the cellphone is much smaller than average APS camera from Table 3; the sensor area of the cellphone camera (23.11mm<sup>2</sup>) is only 6.8% of the average APS sensors (338 mm<sup>2</sup>). In addition, the size of the pixels in a cellphone camera, 2.2×2.2μm, is also much smaller than the pixels in the three APS from Table 3 (6.47×6.47μm). If the number of defects developed in a sensor were proportional to the sensor size, we would expect these cellphone cameras to have defect rate much lower than the DSLRs, substantially less than 1 defects/year. Thus we would not expect to see a significant increase in defect numbers. If we scale area the of the cellphone sensor to the same sensor size as those DSLRs in Table 3, the 8.3 defects/year interpret to 122 defects/years in DSLRs. Note this rate of 122 defects/year is 33 times higher the observed DSLR rate of 3.7 defects/year. Hence, the cellphone small sensor is showing a much larger defect growth than expect on the basis of DSLRs. The high defect rate in cellphone cameras strongly suggests that the small pixel size may experience more defects in these sensors.

Now consider one possible cause of higher defects with smaller pixels. The average pixel area of DSLRs from Table 3 is ~43.6μm<sup>2</sup>. Assuming all pixels have the same efficiency and same optical system is used, the small pixels from cellphone camera (4.8μm<sup>2</sup>) only collect 11% of the light as compare to the large pixels. Thus for the small pixel to create similar output,  $m$  from Equation (1) must increase proportionally. As the scaling factor  $m$  increases, the impact of defect,  $I_{Offset}$ , as calculated from Equation (2) will increase; therefore a hot pixel which was consider weak in a large pixel is much more visible in smaller pixel at the moderate ISO level. DSLR pixel area is 8 times that of the cellphone cameras pixel areas; thus  $I_{Offset}$  will scale by factor of 8 as well which suggested the behavior we observed at ISO 400 from the cellphone camera should be similar to those we observed at the level of ISO 3200 from DSLRs. This is in agreement with our previous studies<sup>2</sup> which showed the size of defect creating the hot pixel is very small (<0.07 μm) which is well within the 2.2 μm pixel size. Since the hot pixel dark current from a given defect remains the same as pixels shrink, but the sensitivity of the pixel to each electron increases, this means that even weak hot pixel like damage causes a significant effect in smaller pixels. However while this could explain a factor of about 8 in the growth rate, it cannot be the only thing happening to get that 33 times increase. The problem is that although  $I_{Offset}$  scales with ISO as shown in Table 2 the increase in defect in umbers is typically less than the change from this expanded ISO. Hence the

8.3 defects/year from cellphone camera is significantly higher than expected and beyond the observed defect rate from DSLRs at higher ISO with a larger sensor and pixels. We need to monitor these cellphone cameras over a longer period of time to gain more insight into the cause of the high defect rate. One caveat here is that while this test covered 10 cameras they were from the same manufacturer and probably the same product batch, so we need to test this on a wider set of cameras with smaller pixels. However, it is an important trend to note not only for the cell phones, but as the drive to more pixels in regular and higher end DSLR cameras causes manufacturers to look at smaller pixels, the impact of defects on these small pixels will be a significant drawback on image quality.

## 5. CONCLUSIONS

In our on-going study of 21 semi-professional cameras, we have observed 243 hot pixels, of which 78% were partially stuck defects. The in-field defects we have observed over the sensor lifetime were permanent and their number increased continuously. In this paper we have emphasized the effect of ISO amplification on defects, and found that the majority of defects found in larger area DSLRs are low impact defects, with small dark current. With the increase of amplification required for the high ISO settings, the distinction between background noise and the defects becomes more significant as more low impact defects can be identified. Based on an analysis of 13 cameras, we have identified a total of 292 defects at ISO 1600, which is 3 times the number of defects found at ISO 400. With a better understanding of the pixel behavior at various ISO settings, we have improved the pixel model in our automated defect trace algorithm, and have applied the algorithm to estimate the defect growth rate for 6 of the cameras. The comparison between DSLRs with different sensor areas but similar pixel sizes showed a much higher defect rate for larger area sensors. This suggests that the number of defects developed is at least proportional to the sensor area.

To study the impact of reducing pixel size we also analyzed a set of cellphone cameras and observed a defect growth rate of 8.3 defects/years. Cellphone cameras have a tiny fraction of the sensor area of DSLRs, and the higher defect rate suggests that the impact of defects is more significant on smaller pixels at the same ISO. As the pixel size decreases, the pixel becomes more sensitive to hot pixel dark currents and the impact of the defect source becomes more significant compared to that in the larger pixels.

We conclude that hot pixels will become a much larger issue in the near future. With more high-end DSLRs moving toward larger area sensors and higher ISO ranges, we will be observing more defects which the amplification due to higher ISO and the offset value of many hot pixels will cause to appear over all exposure times. More importantly, with the shrinkage of pixel size, low impact defects will become more prominent.

## REFERENCES

- [1] J. Dudas, L.M. Wu, C. Jung, G.H. Chapman, Z. Koren, and I. Koren, "Identification of in-field defect development in digital image sensors," *Proc. Electronic Imaging, Digital Photography III*, v6502, 65020Y1-0Y12, San Jose, Jan 2007.
- [2] J. Leung, G.H. Chapman, I. Koren, and Z. Koren, "Statistical Identification and Analysis of Defect Development in Digital Imagers," *Proc. SPIE Electronic Imaging, Digital Photography V*, v7250, San Jose, Jan 2009.
- [3] J. Leung, G. Chapman, I. Koren, and Z. Koren, "Automatic Detection of In-field Defect Growth in Image Sensors," *Proc. of the 2008 IEEE Intern. Symposium on Defect and Fault Tolerance in VLSI Systems*, pg. 220-228, Boston, MA, Oct. 2008.
- [4] J. Leung, G. H. Chapman, I. Koren, Z. Koren, "Characterization of Gain Enhanced In-Field Defects in Digital Imagers," *Proc. of the 2009 Intern. Symposium on Defect and Fault Tolerance in VLSI*, pg 155-163., Chicago, IL, Oct 2009.
- [5] J. Leung, J. Dudas, G. H. Chapman, I. Koren, Z. Koren, "Quantitative Analysis of In-Field Defects in Image Sensor Arrays," *Proc. of the 2007 Intern. Symposium on Defect and Fault Tolerance in VLSI*, pg. 526-534, Rome, Italy, Sept 2007.
- [6] A.J.P. Theuwissen, "Influence of terrestrial cosmic rays on the reliability of CCD image sensors. Part 1: experiments at room temperature," *IEEE Transactions on Electron Devices*, Vol. 54 (12), pg. 3260-6, 2007.
- [7] A.J.P. Theuwissen, "Influence of terrestrial cosmic rays on the reliability of CCD image sensors. Part 2: experiments at elevated temperature," *IEEE Transactions on Electron Devices*, Vol. 55 (9), pg. 2324-8, 2008.